IFIC/91-7
FTUV/91-7

SEMIPHENOMENOLOGICAL APPROACH TO NUCLEON PROPERTIES IN NUCLEAR MATTER

P. Fernández de Córdoba and E. Oset

Departamento de Física Teórica and IFIC,
Centro Mixto Universidad de Valencia CSIC,
46100 Burjassot (Valencia) Spain.

Abstract

We have evaluated the nucleon selfenergy in a model that has proper analytical properties, satisfies the low density theorem and provides values of $\mathrm{Im}\Sigma$ for high densities comparable to those of realistic microscopic approaches. The model, however, relies only upon the NN experimental cross sections and the empirical spin-isospin interaction, which induces an important polarization of the medium. The results obtained for the spectral functions, occupation numbers and effective masses are quite reasonable. However, the sharp peak of the ω and effective masses found in approaches relying in central potential models is not found here. We discuss this point and show the importance of performing realistic microscopical calculations incorporating tensor forces, satisfying the low density theorem and considering the polarization of the medium. The model does not give the absolute value of the nucleon selfenergy but only differences with respect to the Fermi energy. On the other hand it provides an easy and efficient way of evaluating many of the nucleon properties in the nuclear medium.

1.- INTRODUCTION

The nucleon properties in nuclear matter have been thoroughly studied microscopically with several levels of approximation (see ref.[1] for a review). Most calculations rely upon the second order Brueckner Hartree Fock expansion[1], although some steps leading to selfconsistent schemes have been given[2,3]. Non perturbative schemes as the hypernetted chain have also brought their share of progress to the field[4]. With this welth of microscopic work one can wonder what new information can bring along a semiphenomenological analysis. The answer can come from several viewpoints. On the one hand it is interesting to trace back the origin of several nucleon properties to measurable magnitudes of the nucleon-nucleon interaction, such as the scattering cross section, rather than to the nucleon-nucleon interaction itself through the black box of involved many body calculations. On the other hand one can make use of the low density theorems for the nucleon selfenergy and implement them automatically in the semiphenomenological scheme. This guaranties that the low density regime is accurately given, which is by no means true in many microscopical calculations. Finally in many applications in Nuclear Physics one needs only partial information about the nucleon properties which can be easily provided by this semiphenomenological model without the need to recur to sophisticated and elaborate calculations.

With the model we will be able to calculate nucleon properties in nuclear matter as effective masses, imaginary part of the nucleon selfenergy, spectral functions, occupation numbers etc. However we renounce from the beginning to obtain the absolute value of the real part of the nucleon selfenergy, and the nuclear binding as a consequence. This piece of information is more deeply tied to details of the nucleon-nucleon interaction and escapes our simplified analysis. In the study of many nuclear processes this information is however unnecessary since the nucleon selfenergy enters only through differences of selfenergies for two nucleon lines and such information can still be provided by the

semiphenomenological model.

2.- THE LOW DENSITY THEOREM FOR THE NUCLEON SELFENERGY.

At low nuclear densities, ρ, we can make use of an important property which relates the nucleon selfenergy with the NN elementary scattering amplitude. The theorem states that the nucleon selfenergy in nuclear matter is given by [5,6]

$$\Sigma(k^o, \vec{k}) = t(k^o, \vec{k})\rho \qquad (1)$$
$$\rho \to 0$$

where t is the average over the Fermi sea and spin of the forward scattering matrix for the collision of the nucleon with momentum $(k^o, \vec{k})$ and a nucleon of the Fermi sea.

The normalization of the invariant t matrix is such that the NN cross section is given by

$$\frac{d\sigma}{d\Omega} = \frac{1}{4\pi^2} \frac{M^4}{s} \bar{\sum} \sum |t|^2 \qquad (2)$$

with M the nucleon mass, and $s = (p_1 + p_2)^2$ (p_1, p_2 momenta of the initial nucleons). We obtain an interesting consequence of eq. (1) by taking its imaginary part

$$\mathrm{Im}\,\Sigma(k^o, \vec{k}) = \mathrm{Im}\,t(k^o, \vec{k})\rho$$
$$= -\frac{2k_{CM}\sqrt{s}}{2M\,2M}\,\sigma_{tot}\,\rho = -\frac{k}{2M}\,\sigma_{tot}\,\rho = -\frac{1}{2}\,\sigma_{tot}\,v\,\rho \qquad (3)$$

with v the velocity of the particle and σ_{tot} the total NN cross section. In eq. (3) we have used the optical theorem and the fact that $k_{CM} = k\,M/\sqrt{s}$, assuming the nucleons of the Fermi sea at rest.

Eq. (3) puts an important constraint on Σ providing a model independent limit which is easy to check. Most models used in the literature violate this theorem, at some point, because of the approximate NN potentials used or because of the approximations used in the solution of the many body problem. The work of refs.[2,3] is one example of it. Indeed, relying upon the central part of the NN interaction and neglecting tensor forces, as one increases the nucleon energy the NN cross section is progressively underestimated[7].

The test of eq. (3) is very useful since it allows us to have an idea of the accuracy expected from a theory or the kinematical regions where the results are unreliable.

There is another point worth mentioning. As we see, in eq. (3) we have the total NN cross section. At nucleon momenta beyond 1 GeV/c the pion production inelastic channels open up and the NN cross section contains a fair amount of inelastic cross section. Pion production can also proceed with only one nucleon, provided we have off shell nucleon energies, above the pion mass. While this channel is considered in evaluations of the Δ selfenergy[8], it is usually neglected in evaluations of the nucleon selfenergy which rely upon static NN potentials. Eq. (3) certainly requires the inclusion of this channel as soon as the energy allows it. However one must be aware that for some practical applications the inclusion of this channel might be relatively irrelevant. Indeed, for pion scattering the region of energies where pion production is allowed is dominated by the Δ resonance and the nucleon pole terms are very small. One might think that in electronuclear processes, where one can single out the longitudinal response function and exclude the Δ channel, the π production channel will be important. While this is certainly true, the question is that pion excitation by virtual photons not only proceeds through $N \rightarrow N\pi$ or $NN \rightarrow NN\pi$ steps, but there are direct $\gamma N \rightarrow \pi N$ terms, like the pion pole and Kroll Ruderman terms, which are dominant at low pion energies and which can not be cast in terms of the nucleon selfenergy. This is visualized in fig. 1.

Instead of including pion production in the nucleon selfenergy it is more practical to look globally at the pion electroproduction process by means of the diagram of fig. 1d where the dashed circle stands for all terms contributing to $\gamma N \rightarrow \pi N$. This example shows us that the input in the nucleon selfenergy has to be looked at in the context of the physical process that one wants to study. With this in mind we shall also exclude the pion production channels from our model and remember that we have to deal explicitly with this degree of freedom in whichever process we wish to apply the model.

3.- MODEL FOR THE NUCLEON SELFENERGY.

The diagramatic meaning of eq. (1) is given in fig. 2, where the Lippmann Schwinger series leading to the NN t matrix is shown explicitly. Diagram a) does not contribute to the imaginary part of Σ, while all the others do. In order to evaluate it we concentrate in diagram 2b. The selfenergy for this diagram is given by

$$-i\Sigma(k) = \int \frac{d^4q}{(2\pi)^4}\, i\left\{ \frac{1-n(\vec{k}-\vec{q})}{k^o-q^o-\varepsilon(\vec{k}-\vec{q})+i\epsilon} + \frac{n(\vec{k}-\vec{q})}{k^o-q^o-\varepsilon(\vec{k}-\vec{q})-i\epsilon} \right\} \tag{4}$$

$$(-i)\,V(q)\,(-i)\,V(q)\; i\,U_N(q)$$

where the curled bracket accounts for the nucleon propagator, $G(k-q)$, with $\varepsilon(\vec{k})$ the nucleon kinetic energy, and we assume that the NN interaction, $V(q)$, depends only on the momentum transfer for simplicity. $U_N(q)$ is the Lindhard function for ph excitation with the normalization given in the appendix of ref.[9]. In order to obtain the imaginary part we first perform the q^o integration by means of a Wick rotation as shown in fig. 3, which shows the pole structure of the integrand of eq. (4). The crosses correspond to the poles of the Lindhard function and even if $V(q)$ was assumed non static (q^o dependence) it would have the structure of a propagator and the poles

would be like those of $U_N(q)$.

The integral over the circuit of fig. 3 leads to

$$\int_{-\infty}^{\infty} dq^o + \int_{i\infty}^{-i\infty} dq^o = 2\pi i R(k^o - \varepsilon(\vec{k}-\vec{q}))\,\Theta(k^o - \varepsilon(\vec{k}-\vec{q}))(1-n(\vec{k}-\vec{q})\ \text{term})$$

$$-2\pi i R(k^o-\varepsilon(\vec{k}-\vec{q}))\,\Theta(\varepsilon(\vec{k}-\vec{q})-k^o)(n(\vec{k}-\vec{q})\ \text{term}) \qquad (5)$$

The integral over the imaginary axis gives a real contribution to $\Sigma(k)$ since there are cancellations of the imaginary parts of the integral for the positive and negative values of the axis. Thus we obtain:

$$\mathrm{Im}\,\Sigma(k) = \mathrm{Im}\int \frac{d^3q}{(2\pi)^3}\left\{\left(1-n(\vec{k}-\vec{q})\right)\Theta(\vec{k}^o-\varepsilon(\vec{k}-\vec{q})) - n(\vec{k}-\vec{q})\Theta\left(\varepsilon(\vec{k}-\vec{q})-k^o\right)\right\}$$

$$\cdot V(q)^2\,U_N(q)\Big|_{q^o=k^o-\varepsilon(\vec{k}-\vec{q})} \qquad (6)$$

$$= \int \frac{d^3q}{(2\pi)^3}\left\{(1-n(\vec{k}-\vec{q}))\,\Theta(k^o-\varepsilon(\vec{k}-\vec{q})) - n(\vec{k}-\vec{q})\Theta(\varepsilon(\vec{k}-\vec{q})-k^o)\right\}$$

$$\cdot V(q)^2\,\mathrm{Im}\,U_N(q)\Big|_{q^o=k^o-\varepsilon(\vec{k}-\vec{q})}$$

where, since we renounce to include the pionic channels, the only source of imaginary part comes from $U(q)$. As we can see we obtain an imaginary part with the factor $1 - n(\vec{k}-\vec{q})$ when $k^o > \varepsilon_F$ and another one with the factor $n(\vec{k}-\vec{q})$ when $k^o < \varepsilon_F$. The reason why the two contributions come together in our scheme is because $U_N(q)$ accounts for forward and backward ph excitation as shown in fig. 4. As a consequence the two conventional diagrams[1], polarization, fig. 5a, and correlations, fig. 5b, are automatically accounted for in our scheme.

Next we calculate the imaginary part of the selfenergy associated

to diagrams c), d) etc. Note that by means of the Wick rotation we have placed on shell the intermediate nucleon line, through the pole of the nucleon propagator, (eq. (5)), and the ph excitation, through Im $U_N(q)$ in eq. ((6). This is the manifestation of Cutkosky rules which tell us that the imaginary part of the selfenergy is obtained when the particles cut by a horizontal line are placed on shell (see fig. 6). The series of cuts shown in fig. 6 can be reordered in the way shown in fig. 7. We then observe that by summing the diagrams in arrows we generate the t matrix in the upper part of the cut, while summing over columns we generate the t matrix in the lower part of the cut. Hence, the sum of all these diagrams is easily taken into account by simply replacing $V(q)$ in eq. (6) by the t matrix. Analytically this is obtained by means of the relationship

$$\mathrm{Im}(V + VGV + VGVGV + \ldots\ldots) =$$

$$(V + VGV + VGVGV + \ldots\ldots)^*\ \mathrm{Im}\,G\ (V + VGV + VGVGV + \ldots\ldots) \qquad (7)$$

where G is the only source of imaginary part, which in our case corresponds to the Lindhard function. The only novelty with respect to the conclusion from the diagramatic expansion is that one of the T matrices appears complex conjugate. This is indeed one of the prescription of the Cutkosky rules which have its heart in the optical theorem[10].

Hence we obtain for the imaginary part of the nucleon selfenergy the result

$$\mathrm{Im}\,\Sigma(k) =$$

$$= \int \frac{d^3q}{(2\pi)^3}\left\{\left(1-n(\vec{k}-\vec{q})\right)\Theta(k^o-\varepsilon(\vec{k}-\vec{q})) - n(\vec{k}-\vec{q})\Theta(\varepsilon(\vec{k}-\vec{q})-k^o)\right\}$$

$$\mathrm{Im}\,U_N(q)\ \ \bar{\Sigma}\Sigma|t|^2\Big|_{q^o=k^o-\varepsilon(\vec{k}-\vec{q})} \qquad (8)$$

where we have also included the sum and average of $|t|^2$ over final and initial polarizations. One of the initial nucleon states is the hole state of the Lindhard function and we should sum, not average over its spin. The factor two of spin is included in U_N and hence we average $|t|^2$.

So far the derivation is rigorous. The t matrix corresponds to the diagramatic series implicit in fig. 2, with the nucleon propagators containing both particle and hole parts, as the curled bracket of eq. (4). This leads to a t matrix different than the free one, which is the Galitskii t matrix[11,12]. In most studies in the Literature only the particle part of the propagator is taken and one obtains then the Bethe-Goldstone G-matrix. However, the approach of refs.[2,3] relies upon the Galitskii equation. One of our approximations is to take t of eq. (8) as the free NN t matrix. Another one is to substitute $|t|^2$ by its average over angles relating it to the NN cross section by means of the relationship, based on eq. (2)

$$\bar{\sum}\sum |t|^2 \longrightarrow \frac{\pi s}{M^4}\,\sigma_{elas} \simeq \frac{4\pi}{M^2}\,\sigma_{elas} \qquad (9)$$

where σ_{elas} is the elastic NN cross section averaged over isospin, since $U_N(q)$ also contains a factor 2 for isospin. The last step in eq. (9) is made for consistency with other nonrelativistic approximations made in the Lindhard function, etc. At the heart of the replacement of the Galitskii t matrix by the free t matrix is the fact that as $\rho \longrightarrow 0$ they coincide and that by including the contribution of holes the Galitskii equation does not restrict the phase space so much as the Bethe-Goldstone equation and leads to closer results to the free t matrix than the Bethe-Goldstone G-matrix. The density modifications to this formula will come in our approach from the medium polarization, which at low energies plays a very important role.

We have taken the results for σ_{elas} from the particle data tables and we take it dependent on the Mandelstam variable s. When $s<4M^2$,

where evidently there is no scattering, but $|t|^2 \neq 0$, we have taken the value of σ_{elas} for $s = 4M^2$.

At his point we would like to raise a word of caution not to use eq. (4), for the second order diagram, to evaluate the real part of the nucleon selfenergy by replacing V(q) by the t matrix, as we have done to calculate Im Σ. This would lead to doublecounting since two interaction lines on the upper part of the diagram and one in the lower will be counted twice when we consider also one interaction line in the upper part and two in the lower. There was not doublecounting in the imaginary part because the cut giving rise to Im Σ could be placed between any two interaction lines (see figs. 6 and 7).

It is instructive to see that our approximation satisfies exactly the low density theorem. Indeed, as $\rho \to 0$ we can take $n(\vec{n}-\vec{q}) = 0$ in eq. (8) and by means of the useful approximation

$$\Theta(q^o)\,\mathrm{Im}\,U_N(q) \underset{\rho \to 0}{\approx} -\pi\rho\,\delta(q^o - \vec{q}^{\,2}/2M) \qquad (10)$$

and the change of variable $\vec{q} = \vec{q}' + \vec{k}/2$ we perform inmediately the integral in eq. (8) with the result given in eq. (3) for on shell nucleons ($k^o = \vec{k}^{\,2}/2M$). The only difference is that we obtain σ_{elas} instead of σ_{tot}, because, as discussed above, we renounce to incorporate the pion production channels in our approach.

Eq. (8) gives us Im $\Sigma(k)$ also for the case where the original nucleon is off shell ($k^o \neq \vec{k}^{\,2}/2M$). We have to give a prescription on how to evaluate t when the initial nucleon is off shell. This requires the knowledge of the dynamics of the NN interaction. If we think in terms of meson exchange models for the interaction we would have a form factor F(q) in each of the four vertices in the diagram of fig. 2b. In an off shell situation q^2 would change with respect to the on shell value q^2_{on} and by multiplying σ by $(F(q)/F(q_{on}))^4$ we would account for the off shell effects due to the

vertices. The propagators would also change. However, it is easy to prove that if we assume the hole line in the Lindhard function to have as an average a momentum $p_2 = (m, \vec{0})$, we can also make an average for the longitudinal component of $\vec{q}$ along the $\vec{k}$ direction which provides $q_L = k/2$. Then we find the average value of $\vec{q}^2 = Mk^o$ and $q^o = \vec{q}^2/2M$ irrespective of whether $(k^o, \vec{k})$ is on shell or off shell. Then our prescription is very clear: for any off shell situation, $(k^o, \vec{k})$, we take the cross section σ corresponding to the on shell situation, $(k^o, k = \sqrt{2Mk^o})$.

The scheme which we have developed has as a main virtue to satisfy the low density theorem, but it automatically provides an analytical extrapolation of these results to finite densities, incorporating Pauli blocking effects through the Lindhard function and the two terms of eq. (8). It also provides an off shell extrapolation, through the explicit dependence of eq. (8) on k^o and $\vec{k}$. It has also the appropriate analytical properties, $\mathrm{Im}\,\Sigma(k)$ vanishes at $k^o = \varepsilon_F = k_F^2/2M$ and is negative for $k^o > \varepsilon_F$ and positive for $k^o < \varepsilon_F$, as demanded by general theorems[14]. However, as shown in ref.[9], for densities $\rho = \rho_o$, $\rho_o/2$ (ρ_o normal nuclear matter density) and $k^o = \varepsilon_F + 85$ MeV the present scheme provides $\mathrm{Im}\,\Sigma \simeq -10.4$ MeV, -7.2 MeV, versus the value -6.5 MeV both for ρ_o and $\rho_o/2$ provided by the microscopic calculations of ref.[4]. This reflects the fact that at higher densities there are quenching mechanisms beyond Pauli blocking which further reduce the results from the scheme exposed above.

It is interesting to recall the basic ingredients incorporated in the hypernetted chain approach of ref.[4]. From the diagramatic point of view it incorporates ladder sums, which we have already summed in the t matrix, and polarization sums obtained by allowing the interaction to excite ph components in an iterative way. This is shown diagramatically in fig. 8. We wish to include these effects in our scheme and we do this in the next section.

4.- POLARIZATION EFFECTS.

In order to include the polarization effects of fig. 8 we must perform the geometric series implicit in the figure and there we need the ph interaction. Here again we adopt a phenomenological approach. At energies of the nucleon $k^o > \varepsilon_F + 50$ MeV the value of q exceeds 200 MeV/c. This momenta are already bigger than the pion mass and make the tensor force of the NN interaction appreciable. Our position here is that at these energies the ph interaction is dominated by the spin-isospin effective interaction and we shall use this one for the iteration of the ph excitation in fig. 8. This interaction is given by

$$V_{s-i}(q) = \left\{ V_l(q)\,\hat{q}_i\hat{q}_j + V_t(q)(\delta_{ij} - \hat{q}_i\hat{q}_j) \right\} \sigma_i\sigma_j\,\vec{\tau}\,\vec{\tau} \qquad (11)$$

with

$$V_l(q) = \frac{f^2}{m_\pi^2}\left[\frac{\vec{q}^2}{q^{o2} - \vec{q}^2 - m_\pi^2}\,F_\pi^2(q) + g'\right]$$

$$V_t(q) = \frac{f^2}{m_\pi^2}\left[\frac{\vec{q}^2}{q^{o2} - \vec{q}^2 - m_\rho^2}\,F_\rho^2(q)\,C_\rho + g'\right] \qquad (12)$$

where $F_i(q)$ is the meson-NN form factor which we take of the monopole type $F_i(q) = (\Lambda_i^2 - m_i^2)/(\Lambda_i^2 - q^2)$ with $\Lambda_\pi = 1300$ MeV, $\Lambda_\rho = 1400$ MeV[15]. C_ρ is the ratio of squares of ρNN and πNN coupling constants, for which we take $C_\rho = 3.94$ from ref.[15] and $f^2/4\pi = 0.08$. Finally g' is the Landau-Migdal parameter for which we take $g' = 0.7$ in our calculations. Accounting for the geometrical series is trivial and we obtain two independent series, one for the longitudinal part, V_l, and another one for the transverse part, V_t. However, due to the smallness of the ρ-meson contribution in V_t, this term is approximately equal to g', while in the longitudinal part, due to the smallness of the pion mass there are cancellations between the pion exchange contribution and g' and then V_l is small compared to V_t. We

hence assume for simplicity that the ph excitation is driven by the transverse part alone and then the whole series leading to the induced interaction[16] of fig. 8 is accounted for by replacing in the formulas

$$U_N(q) \longrightarrow \frac{U_N(q)}{1 - V_t(q)\, U_N(q)} \tag{13}$$

However since in $\mathrm{Im}\,\Sigma(k)$ what we needed is $\mathrm{Im}\,U_N(q)$, the replacement to be made in eq. (8) is

$$\mathrm{Im}\,U_N(q) \longrightarrow \mathrm{Im}\,\frac{U_N(q)}{1 - V_t(q)\, U_N(q)} = \frac{\mathrm{Im}\,U_N(q)}{\left|1 - V_t(q)\, U_N(q)\right|^2} \tag{14}$$

The last step in this process is that with the spin-isospin interaction one can also excite Δh components. We can easily account for that by replacing $U_N(q)$ by $U(q) = U_N(q) + U_\Delta(q)$, with $U_\Delta(q)$ incorporating ratios of coupling constants and spin-isospin factors and normalized as in ref.[9]. However, since the source of $\mathrm{Im}\,U_\Delta(q)$ is the decay $\Delta \rightarrow \pi N$ and we neglect this channel here (we also neglect other sources of $\mathrm{Im}\,U_\Delta(q)$ studied in ref.[8] and which would lead to 3p 2h excitation in the nucleon selfenergy) the final prescription is to substitute

$$\mathrm{Im}\,U_N(q) \longrightarrow \frac{\mathrm{Im}\,U_N(q)}{\left|1 - V_t(q)\, U(q)\right|^2} \tag{15}$$

Hence Δh excitation does not contribute directly to $\mathrm{Im}\,\Sigma$ because we omit the pion creation channel, but the virtual Δh excitation plays an indirect role through the medium polarization.

The consideration of the polarization brings our results for $\mathrm{Im}\,\Sigma$ in close agreement with the results of ref.[4] as we shall see in the results section.

5.- THE REAL PART OF THE NUCLEON SELFENERGY.

We can of course take eq. (1) and rely upon the free NN

elementary amplitude in order to obtain the low density limit. The high density limit would require the use of the Galitskii t matrix, although higher orders and a selfconsistent treatment also have some influence in the results[2]. This is one of the magnitudes where the details of the interaction matter most. Indeed the strong repulsion at short distances would make this magnitude even change sign at sufficiently high densities. We renounce to have all the information on $\mathrm{Re}\,\Sigma$, but as we shall see we can obtain the relevant information to evaluate a great deal of nuclear properties relying again on the same phenomenological input used so far.

Since our results for $\mathrm{Im}\,\Sigma$, fulfilling the low density theorem and in agreement with the results of ref.[4] for high densities, are sufficiently realistic, we can use a dispersion relation to obtain the real part from the imaginary part. Considering the analytical structure of our selfenergy we obtain[1,2]

$$\mathrm{Re}\,\Sigma(\omega, k) = -\frac{1}{\pi}\, P\int_{\varepsilon_F}^{\infty} d\omega'\, \frac{\mathrm{Im}\,\Sigma(\omega', k)}{\omega - \omega'} + \tag{16}$$

$$+ \frac{1}{\pi}\, P\int_{-\infty}^{\varepsilon_F} d\omega'\, \frac{\mathrm{Im}\,\Sigma(\omega', k)}{\omega - \omega'}$$

With this expression of course we only evaluate the real part associated to the diagrams of figs. 2b, c, d, ... which provide the source of $\mathrm{Im}\,\Sigma$. The Hartree term, fig. 2a and the Fock term, not shown but understood in the series are not taken into account by means of eq. (16) and have to be added explicitly (note that the antisymmetry in the NN amplitude is incorporated phenomenologically in σ for the other terms of the series).

We are interested only in the pieces of $\mathrm{Re}\,\Sigma$ which depend on k^o and k in order to obtain effective masses, strength at the pole etc. This means that we do not need to evaluate the Hartree piece, but the Fock piece gives rise to an important k dependence and we must consider it.

The Fock term is shown diagramatically in fig. 9. The contribution of a static pion exchange ($q^o = 0$) is easily evaluated and we obtain

$$\Sigma^{(F)}(k) = -3 \int \frac{d^3q}{(2\pi)^3}\; n(\vec{k}-\vec{q})\; \frac{f^2}{m_\pi^2}\; \frac{\vec{q}^2}{-\vec{q}^2 - m_\pi^2}\; F^2(q) \tag{17}$$

$$\left\{ k - q \equiv q' \right\} = -3 \int \frac{d^3q'}{(2\pi)^3}\; n(\vec{q}')\; \frac{f^2}{m_\pi^2}\; \frac{(\vec{k}-\vec{q}')^2}{-(\vec{k}-\vec{q}')^2 - m_\pi^2}\; F(k-q')^2$$

We see that the Fock term with a static potential depends on k but not on k^o, it is static. It is also real. This is by contrast to the piece in eq. (16) which depends on both $k^o \equiv \omega$ and k and is tied to pieces which have an imaginary part. The other observation is that the k dependence comes because of the πNN vertex, $\sigma(\vec{k}-\vec{q}')$, leading to the factor $(\vec{k}-\vec{q}')^2$ in the numerator of eq. (17) and because of the pion propagator. If instead of a pion we exchange an ω meson we do not have the derivative coupling (or at least is rather small) and $(\vec{k}-\vec{q}')^2$ in the ω propagator would be weighed against m_ω^2, which is much larger than m_π^2. Hence the dependence on $\vec{k}^2$ of the corresponding Fock piece would be weak. These ideas were discussed in ref.[17] where the sources of k^o and k dependence of the nucleon selfenergy were traced back to the series of terms of figs. 8 and 9 with the spin-isospin part of the nucleon interaction. Hence in order to complete the real part given by eq. (16) we must add the Fock term with the interaction of eq. (11). The result for this piece is

$$\Sigma^{(F)}(k) = -3 \int \frac{d^3q}{(2\pi)^3}\; n(\vec{k}-\vec{q})\,[V_l(q) + 2V_t(q)] \tag{18}$$

Thus, eq. (8) implementing eqs. (9) and (15) for $\mathrm{Im}\Sigma$, together with eqs. (16) and (18) for $\mathrm{Re}\Sigma$ give us the nucleon selfenergy, up to a smoothly k^o, k dependent part, which we disregard.

6.- APPLICATIONS.

a)- Spectral functions.

With the amount of information which we have we can calculate the spectral functions. The Lehmann representation for the nucleon propagator is given by

$$G(\omega, k) = \int_\mu^\infty d\omega' \; \frac{S_p(\omega', k)}{\omega - \omega' + i\eta} + \int_{-\infty}^{\mu} \frac{S_h(\omega', k)}{\omega - \omega' - i\eta} \tag{19}$$

where μ is the chemical potential and S_p, S_h the particle and hole spectral functions.

By comparing it to the Dyson representation

$$G(\omega, k) = \frac{1}{\omega - \left(\vec{k}^2/2M\right) - \Sigma(\omega, k)} \tag{20}$$

one has the relationships

$$\omega > \mu, \quad S_p(\omega, k) = -\frac{1}{\pi}\, \mathrm{Im}\, G(\omega, k) = -\frac{1}{\pi}\; \frac{\mathrm{Im}\,\Sigma(\omega, k)}{A + B}$$

$$A = \left(\omega - \left(\vec{k}^2/2M\right) - \mathrm{Re}\,\Sigma(\omega, k)\right)^2$$

$$B = \left(\mathrm{Im}\,\Sigma(\omega, k)\right)^2$$

$$\omega < \mu, \quad S_h(\omega, k) = +\frac{1}{\pi}\, \mathrm{Im}\, G(\omega, k) = +\frac{1}{\pi}\; \frac{\mathrm{Im}\,\Sigma(\omega, k)}{A + B} \tag{21}$$

The chemical potential in our scheme is given by

$$\mu = \frac{k_F^2}{2M} + \mathrm{Re}\,\Sigma\left(\frac{k_F^2}{2M},\; k_F\right) \tag{22}$$

However the calculations of the selfenergy have been performed assuming only kinetic energies for the nucleon lines. Thus, when the energy

is $k_F^2/2M$, then Im Σ ($k_F^2/2M$, k_F) is zero. The results are invariant if we add a constant real piece to the nucleon energy, because one is always dealing with differences of energies. Hence we can refer the selfenergies to the value at the Fermi surface and define

$$\tilde{\Sigma}(\omega, k) = \Sigma(\omega, k) - \mathrm{Re}\,\Sigma\left(\frac{k_F^2}{2M},\ k_F\right)$$

and as a consequence (23)

$$\tilde{\Sigma}\left(\frac{k_F^2}{2M},\ k_F\right) = 0, \qquad \mu = \frac{k_F^2}{2M}$$

and $\Sigma(\omega, k)$ is calculated using the kinetic energy in the internal nucleon lines as we have done so far.

We can then represent the spectral functions for fixed k as a function of ω, but ω has to be understood as the difference between the actual energy and the exact value of Re $\Sigma(\omega_F, k_F)$. By means of that we eliminate the unknown missing pieces in our approach.

As long as $\Sigma(\omega, k)$ - Re $\Sigma(k_F^2/2M, k_F)$ is small compared to the kinetic energies, ω is approximately the kinetic energy of the particle, and at the Fermi surface ω means exactly the Fermi kinetic energy. In eqs. (20), (21) we would then replace $\Sigma(\omega, k)$ by $\tilde{\Sigma}(\omega, k)$.

b.- Occupation number.

One can easily prove[1, 14] that

$$\langle\psi_o|\, a^+(\vec{k})\, a(\vec{k})\,|\psi_o\rangle = \int_{-\infty}^{\mu} d\omega'\, S_h(\omega', \vec{k})$$

$$\langle\psi_o|\, a(\vec{k})\, a^+(\vec{k})\,|\psi_o\rangle = \int_{\mu}^{\infty} d\omega'\, S_p(\omega', \vec{k}) \qquad (24)$$

o equvalently

$$n(\vec{k}) = \int_{-\infty}^{\mu} d\omega'\, S_h(\omega', \vec{k})$$

$$1-n(\vec{k}) = \int_{\mu}^{\infty} d\omega'\, S_p(\omega', \vec{k}) \qquad (25)$$

which leads to the sum rule

$$\int_{-\infty}^{\mu} d\omega'\, S_h(\omega', \vec{k}) + \int_{\mu}^{\infty} d\omega'\, S_p(\omega', \vec{k}) = 1 \qquad (26)$$

c.- Effective masses and other quasiparticle properties.

We can also evaluate the usual, k, ω and effective masses.

$$\frac{M_\omega}{M} = 1 - \frac{\partial\, \mathrm{Re}\,\tilde{\Sigma}(\omega, \vec{k})}{\partial\omega}\bigg|_{\omega=\omega(\vec{k})}$$

$$\frac{M_k}{M} = \left(1 + \frac{M}{k}\ \frac{\partial\, \mathrm{Re}\,\tilde{\Sigma}(\omega, \vec{k})}{\partial k}\right)^{-1}\bigg|_{\omega=\omega(\vec{k})} \qquad (27)$$

$$\frac{M^*}{M} = \frac{M_\omega}{M}\ \cdot\ \frac{M_k}{M}$$

where $\omega(\vec{k})$ is the quasiparticle energy associated to the momentum $\vec{k}$ given by the solution to the equation

$$\omega - \frac{\vec{k}^2}{2M} - \mathrm{Re}\,\tilde{\Sigma}(\omega, \vec{k}) = 0 \qquad (28)$$

The inverse of M_ω/M is the quasiparticle strength

$$Z(k) = \left[1 - \frac{\partial \, \mathrm{Re}\, \tilde{\Sigma}\,(\omega, k)}{\partial \omega}\right]^{-1}_{\omega = \omega(\vec{k})} \qquad (29)$$

7.- RESULTS AND DISCUSSION.

In fig. 10 we show the results for $\mathrm{Im}\,\Sigma(\omega, k)$ for $k = k(\omega)$, given by the eq. (28), as a function of $\omega - \mu$. We represent the results for two densities, $\rho = \rho_o$ and $\rho = \rho_o/2$. We see that below $\omega - \mu = 60$ MeV $\mathrm{Im}\,\Sigma(\omega, k)$ for $\rho = \rho_o/2$ is bigger than for $\rho = \rho_o$ and above that energy the opposite occurs. This shows the drastic effects of the polarization, together with Pauli blocking, which are more apparent at low energies. The results have been obtained with a value $g' = 0.7$ for the Landau-Migdal parameter. The results in fig. 10 agree remarkably well in magnitude with those of ref.[4] for both densities and the range of energies in the figure. This gives us confidence about the accuracy of the numerical results of the present approach.

In fig. 11 we show the results for M_ω/M as a function of k at $\rho = \rho_o$. While the results are numerically similar to other approaches[1], one feature immediately calls our attention. The peak present in most calculations around the Fermi momentum, $k_F \simeq 1.36$ fm^{-1}, is absent in our approach. A trace of it remains at much lower momenta. The peak around the Fermi surface appears in approaches based in second order perturbation calculations, as reported in ref.[1], or even selfconsistent schemes, but which neglect the polarization of the medium, and rely essentially on central potentials. We have checked that neglecting the polarization changes the results but does not change appreciably the shape of the effective mass. On the other hand we have used an interaction like the one of the model reported in eq. (3. 7. 23) of ref.[1] and performed the calculation. We have replaced in eq. (9)

$$\frac{4\pi}{M^2}\,\sigma_{elas} \rightarrow 3\left(\frac{1}{\vec{q}^{\,2} + m_\pi^2}\right)^2 \qquad (30)$$

which is equivalent to accepting a Yukawa potential as interaction (the factor 3 is introduced to have similar strengths in the two terms). We reproduce the peak in M^*/M as reported in ref.[1]. We tend to conclude that the fact that the central potentials, neglecting tensor forces, provide small NN cross sections at large energies is the main factor responsible for the sharp peak in the effective mass, and that this peak should not be present if realistic calculations, fulfilling the low density theorem at all energies, are used.

In fig. 12 we show the results for M_k/M at $\rho = \rho_o$. The results are similar in shape and size to those of other approaches[1,2]. The smoothness of the curve is the most distinctive feature of this magnitude. Finally in fig. 13 we show the results for M^*/M at $\rho = \rho_o$, which show a flat character around k_F and a fall down at low energies. The effective mass is practically constant and equal to about 0.95 M in a large stretch around k_F. This is compatible with experimental results based on the spacing of levels around the Fermi surface[1,18]. The values of M^* at low energies are also compatible with the level structure of deeply bound states[1]. However, the values of M^* at energies above the Fermi energy would seem to contradict the experimental evidence about the energy dependence of the strength of the potential. This one seems to support $M^* = 0.7$ M at energies $\omega - \mu > 20$ MeV[1]. However, we would like to call the attention at the way that this is obtained. Following ref.[1] we recall that a potential with a Woods Saxon shape is assumed, with a radius slightly larger than the nuclear radius. The strength depends on the energy but the shape is assumed independent of it. We should note that the shape proportional to ρ with a certain finite range is not supported by the present or other calculations which provide a different density functional, also rather energy dependent. Second, the range implemented in the Woods Saxon potential should also be energy

dependent, since, as we increase the energy, p-waves or higher partial waves will become relevant and they give rise to different range corrections in the potential[9,19,20].

The spectral functions show the characteristic features of these functions. In fig. 14 we show $S_p(\omega, k)$ as a function of $\omega-\mu$ for $k > k_F$. We can see that the spectral function ressembles very much a δ function like peak since it corresponds to a Lorentzian distribution with a very narrow width (see eq. (21)). However, in fig. 15 we show $S_p(\omega, k)$ for $k < k_F$. The shape is completely different since S_p is very small and has a long range. The reason for this behaviour is that with $k < k_F$ and $\omega > \mu$ one is far away from the peak of the Lorentzian distribution of eq. (21). (Note different scales in figs. 14 and 15).

The situation is reversed for $S_h(\omega, k)$ which has a pronounced peak for $k < k_F$ (see fig. 16) and is very small and stretches for a long span when $k > k_F$ (see fig. 17).

With the values of the spectral functions we can obtain occupation numbers. In table I we show the occupation number $n(\vec{k})$ and $1-n(\vec{k})$ obtained using eqs. (25), together with the check of the sum rule, which is fulfilled with an average error of three per thousand. We obtain occupation numbers around 0.9 below the Fermi sea and values going down fast from around 0.1 above the Fermi sea. Our results also show the discontinuity of $n(\vec{k})$ around the Fermi surface. For values of $k \approx 1000$ MeV our results become less trustable because of the nonrelativistic treatment, neglect of pion production channels and other approximations done. We can see that in the fact that the integral

$$\frac{3}{k_F} \int_0^\infty dk \; k^2 \, n(k) \qquad (31)$$

which should be unity give values around 1.2 at $k_F = 1.4$ fm^{-1}, coming from the large weight given to large values of k where $n(\vec{k})$ is more unreliable. Note that between $k = 1.45$ fm^{-1} and $k = 3$ fm^{-1} there has been only a

reduction of a factor 2 in the integrand and the integral converges slowly.

It is interesting to recall that the input in our model was the elementary NN cross section and the spin-isospin effective interaction. Any potential model which gave rise to the same NN cross section would lead to the same results in our approach. We find occupation numbers very similar to those obtained in other approaches. The link between the occupation number and short range correlations which has been invoked some times[2] appears unclear in view of the results of the present model which does not require any specific potential.

The approach followed here has the virtue of showing that many of the dynamical properties of nucleon propagation in nuclear matter can be traced to simple dynamical features of the NN interaction reflected in observable magnitudes as cross sections, etc.

8.- CONCLUSIONS.

The approach followed here is semiphenomenological. It starts from a formal derivation of the nucleon selfenergy but at some point relates the input needed of the NN interaction to the NN cross section which is taken from experiment. By means of that are obtains an imaginary part of the nucleon selfenergy which satisfies the low density theorem. Another important ingredient in the approach is the polarization of the medium which produces an appreciable quenching of $\mathrm{Im}\,\Sigma$ at low energies and high densities. The results obtained with these ingredients for $\mathrm{Im}\,\Sigma$ are in good agreement with those of the hypernetted chain approach. With these realistic results for $\mathrm{Im}\,\Sigma$ one evaluates $\mathrm{Re}\,\Sigma$ by means of dispersion relations. This quantity is a dynamical one in the sense that it depends on ω and k as independent variables. To this piece we add a Fock term which is static, and hence depends only on k. This completes the model for the selfenergy which misses some pieces of Hartree type, which depend upon ρ but not on ω or k. Hence the model allows one to obtain all sort of quasiparticle properties which depend upon derivatives of Σ, or other

properties but referred to the variable $\omega-\mu$, since we are unable to evaluate the absolute value of μ.

We have evaluated spectral functions for particles and holes and then occupation numbers with quite acceptable results.

We have also evaluated effective masses. The k-mass has a similar behaviour to most approaches but the ω-mass and, as a consequence, the effective mass, have a different behaviour to most approaches and does not have a sharp peak around the Fermi surface but a rather flat behaviour. The peak seems to be tied to the use of central potentials in standard approaches, which leads to small NN cross sections at high energies. Our approach, relying upon experimental cross sections, incorporates implicitly the effect of tensor forces, which are important at high energies.

The approach can provide many nucleon properties using a minimum amount of experimental information. In this sense it provides some clarification to the problem since in many elaborate many body calculations it is difficult to trace back the results to some basic properties of the interaction. In the other sense it provides a calculational scheme sufficiently realistic and far simpler than other realistic calculations, which can be used in the study of physical processes where the nucleon selfenergy is needed. Finally, the relative flatness of the effective mass around the Fermi energy challenges the results of many calculations. It would be very interesting to perform microscopic calculations incorporating tensor forces, satisfying the low density theorem, and taking care of the polarization of the medium, in order to see whether they support the results obtained here or they are consequence of some of the approximations done.

P. Fernández de Córdoba wishes to acknowledge a fellowship from Ministerio de Educación y Ciencia. This work is partially supported by CICYT.

REFERENCES

1.- C. Mahaux, P.F. Bortignon, R. A. Broglia and C. H. Dasso, *Phys. Reports* **120** (1985) 1.

2.- A. Ramos, A. Polls and W.H. Dickhoff, *Nucl. Phys.* **A503** (1989) 1.

3.- W. H. Dickhoff, P. P. Domitrovich, K. Allaart, M. G. E. Brand, F. Muller, G. Rijnsdijk, A. Polls and A. Ramos, *Proc. Topical Workshop on two nucleon emission reactions*, Elba 1989, in print.

4.- S. Fantoni and V. R. Pandharipande, *Nucl. Phys.* **A427** (1984) 473.

5.- C. B. Dover, J. Hüfner and R. H. Lemmer, *Ann. Phys.* **66** (1971) 248.

6.- J. Hüfner, *Phys. Reports* **21** (1975) 1.

7.- A. Polls, private communication.

8.- E. Oset and L. L. Salcedo, *Nucl. Phys.* **A468** (1987) 631.

9.- E. Oset, P. Fernández de Córdoba, L. L. Salcedo and R. Brockmann, *Phys. Reports* **188** (1990) 79.

10.- C. Itzykson and B. Zuber, *Quantum Field Theory*, McGraw Hill, 1980.

11.- V. M. Galitskii, *Sov. Phys.* JETP, 7 (1958) 104.

12.- A. L. Fetter and J. D. Walecka, *Quantum Theory of many particle systems*, McGraw Hill, 1971.

13.- C. Garcia-Recio and E. Oset, *Phys. Rev.* **C37** (1988) 194.

14.- R. D. Mattuck, *A guide to Feynman diagrams in the many body problem*, McGraw Hill, 1976.

15.- R. Machleidt, K. Holinde and Ch. Elster, *Phys. Reports* **149** (1987) 1.

16.–G. E. Brown, *Many Body Problems*, North Holland, 1972.

17.–E. Oset and A. Palanques, *Nucl. Phys.* **A359** (1981) 289.

18.–G. E. Brown, J. H. Gunn and P. Gould, *Nucl. Phys.* **46** (1963) 598.

19.–A. M. Green and S. Wycech, *Nucl. Phys.* **A377** (1982) 441.

20.–T. Suzuki and H. Narumi, *Phys. Lett.* **B125** (1983) 251; *Nucl. Phys.* **A426** (1984) 413.

FIGURE CAPTIONS.

Fig. 1.– Diagrams entering electron scattering with nuclei leading to pion production. a) $\gamma N \longrightarrow \pi N$ nucleon pole term; b) Kroll Ruderman term; c) pion pole term; d) symbolic representation of all these terms involving the $\gamma N \longrightarrow \pi N$ scattering matrix represented by the dashed circle.

Fig. 2.– Ladder sum for the nucleon selfenergy. The dashed lines indicate a NN potential.

Fig. 3.– Path followed in the Wick rotation used to evaluate eq. (6). The crosses indicate the poles (or rather the analytical cut) of $U_N(q)$.

Fig. 4.– The two diagrams, direct (a) and crossed (b), accounted for by the Lindhard function.

Fig. 5.– Two diagrams leading to Im Σ. a) polarization diagram; b) correlation diagram.

Fig. 6.– The series of fig. 2 showing the sources of ImΣ when the particles cut by the dotted lines are placed on shell in the integrations.

Fig. 7.– Reordering of the series of fig. 6 leading to the last diagram of the figure, where the serrated line indicates the medium t–matrix.

Fig. 8.– Selfenergy diagram including the effects of the medium polarization.

Fig. 9.– The Fock piece of the nucleon selfenergy.

Fig. 10.– Im$\Sigma(\omega, k(\omega))$ as a function of $\omega-\mu$ for two nuclear densities.

Fig. 11.– The ω–mass as a function of k.

Fig. 12.– The k–mass as a function of k.

Fig. 13.– The effective mass as a function of k.

Fig. 14.– $S_p(\omega, k)$ for $k > k_F$ as a function of $\omega-\mu$.

Fig. 15.– $S_p(\omega, k)$ for $k < k_F$ as a function of $\omega-\mu$.

Fig. 16.– $S_h(\omega, k)$ for $k < k_F$ as a function of $\omega-\mu$.

Fig. 17.– $S_h(\omega, k)$ for $k > k_F$ as a function of $\omega-\mu$.

TABLE I

$K_F = 1.40\ fm^{-1}$

$k\ (fm^{-1})$	$n(k)=\int_{-\infty}^{\mu} d\omega\ S_h(\omega,k)$	$1-n(k)=\int_{\mu}^{\infty} d\omega\ S_p(\omega,k)$	Sum
0.1	0.9123	0.0841	0.9964
0.2	0.9152	0.0842	0.9994
0.3	0.9141	0.0847	0.9988
0.5	0.9014	0.0872	0.9886
0.7	0.9097	0.0912	1.000
0.8	0.9073	0.0937	1.001
0.9	0.9041	0.0968	1.000
1.0	0.8978	0.1007	0.9985
1.1	0.8948	0.1056	1.000
1.2	0.8869	0.1117	0.9986
1.30	0.8757	0.1205	0.9962
1.35	0.8522	0.1267	0.9789
1.45	0.1076	0.8599	0.9675
1.5	0.096	0.8925	0.988
1.6	0.079	0.9205	0.999
1.7	0.067	0.9301	0.997
1.8	0.057	0.9374	0.994
1.9	0.054	0.9494	1.003
2.0	0.044	0.9546	0.9986
2.25	0.032	0.9656	0.9976
2.5	0.025	0.9712	0.9962
2.75	0.021	0.9754	0.9964
3.0	0.016	0.9825	0.9985
5.0	0.000		

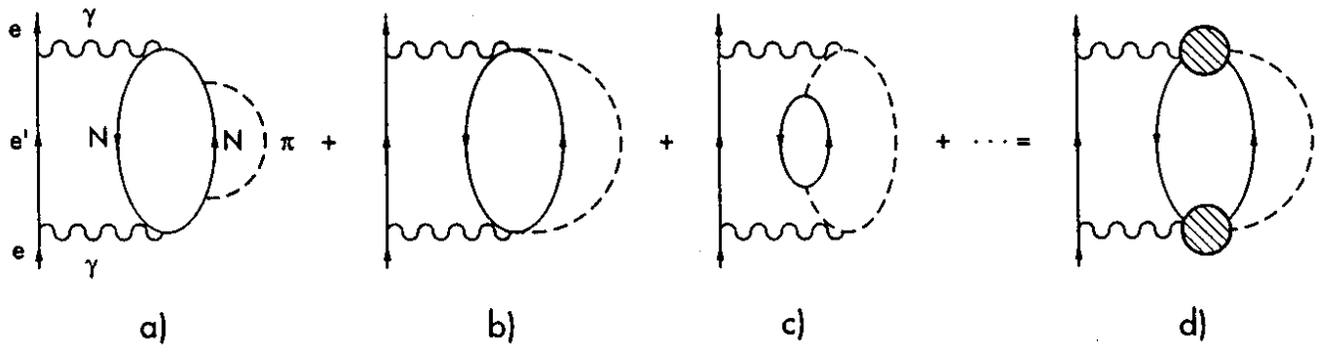

fig. 1

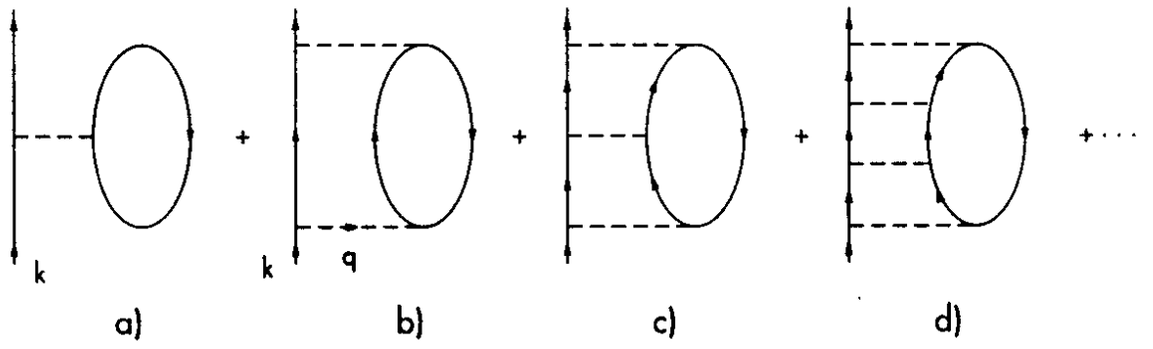

fig. 2

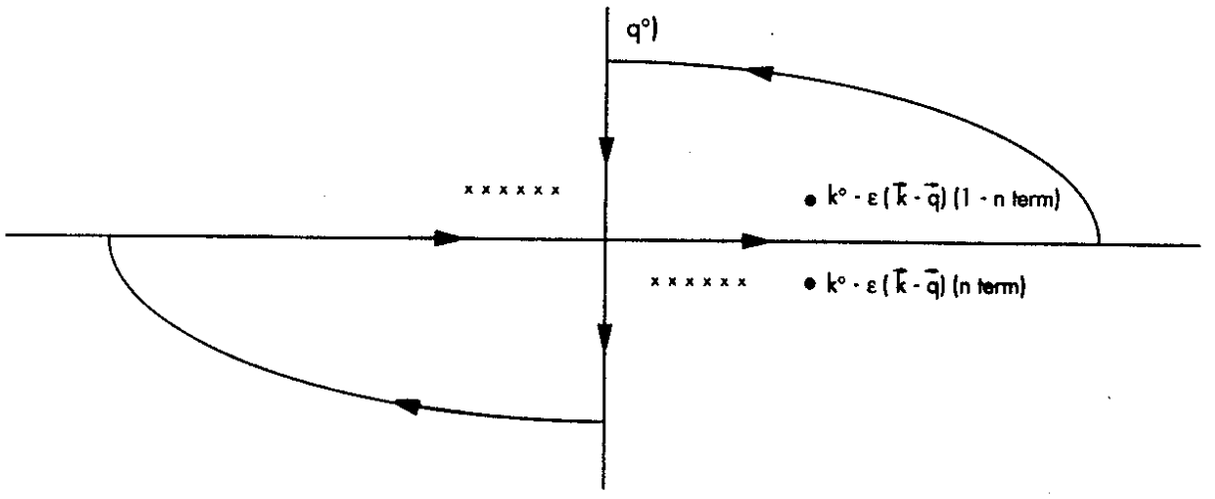

fig. 3

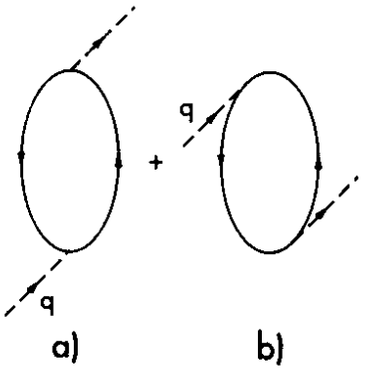

fig. 4

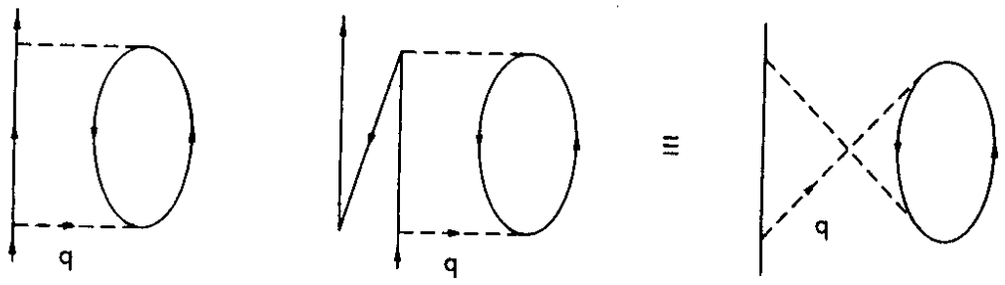

a) b) c)

fig. 5

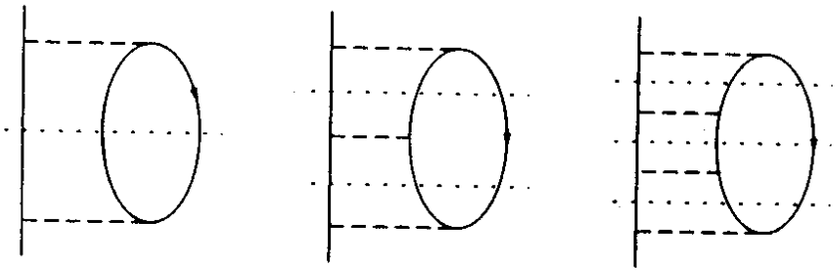

a) b) c)

fig. 6

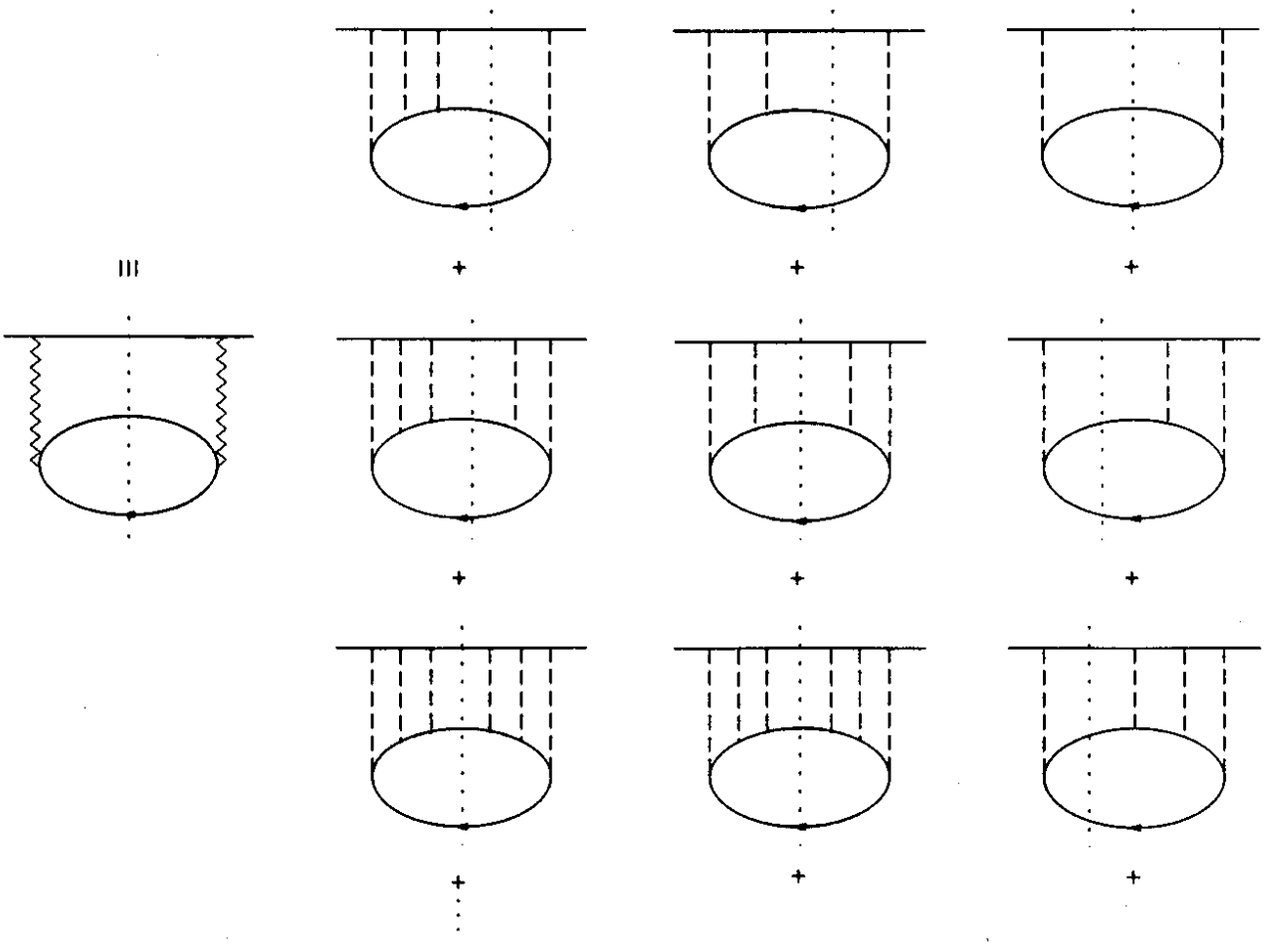

fig. 7

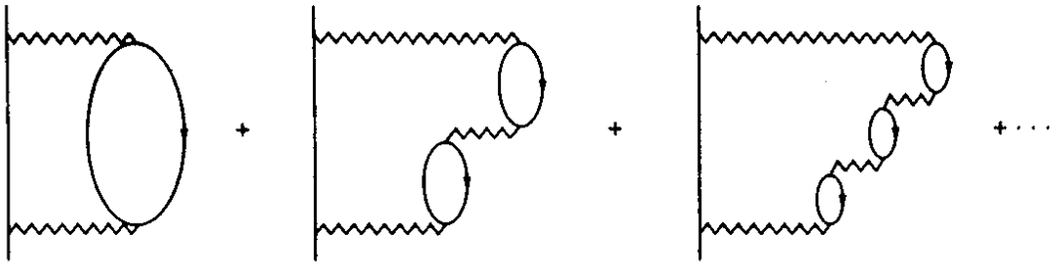

fig. 8

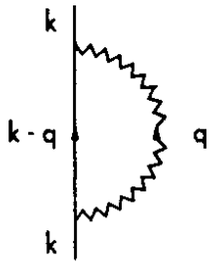

fig. 9

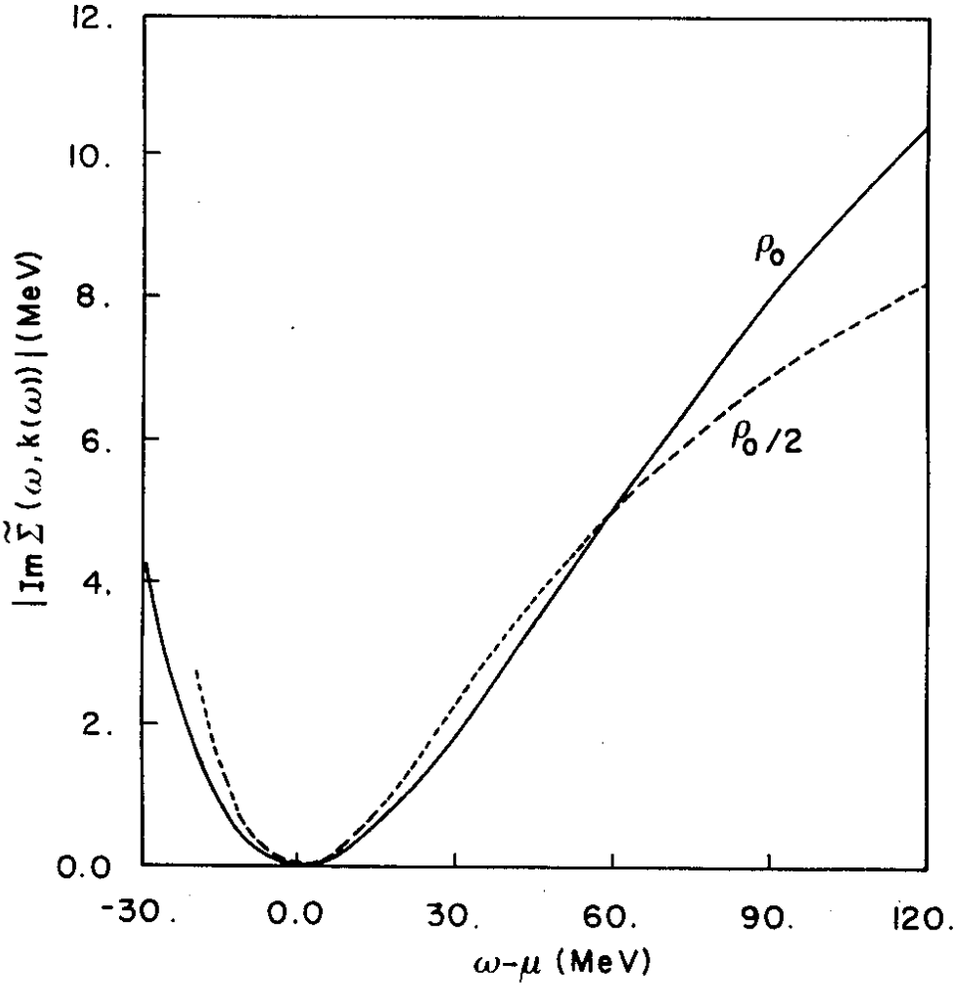

fig. 10

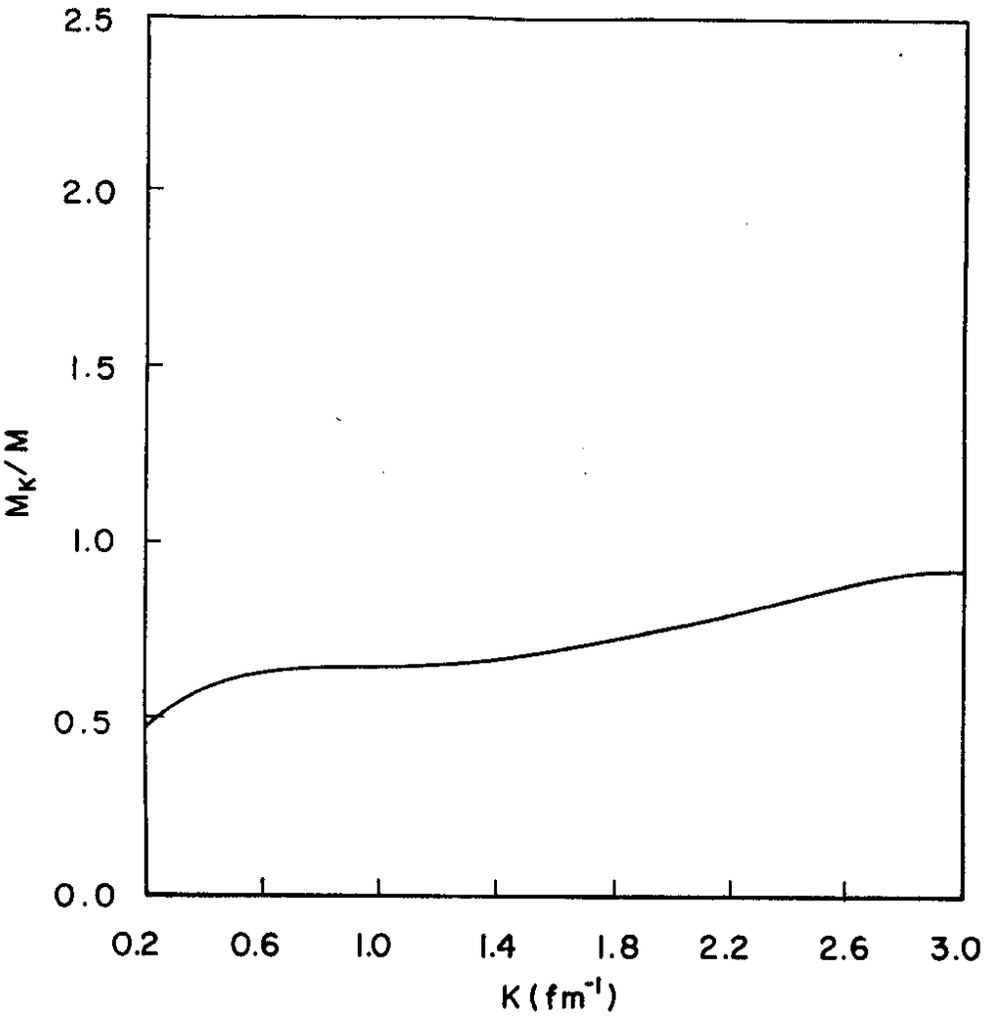
2.5
2.0
1.5
1.0
0.5
0.0
M_K / M
0.2
0.6
1.0
1.4
1.8
2.2
2.6
3.0
$K(fm^{-1})$

fig. 12

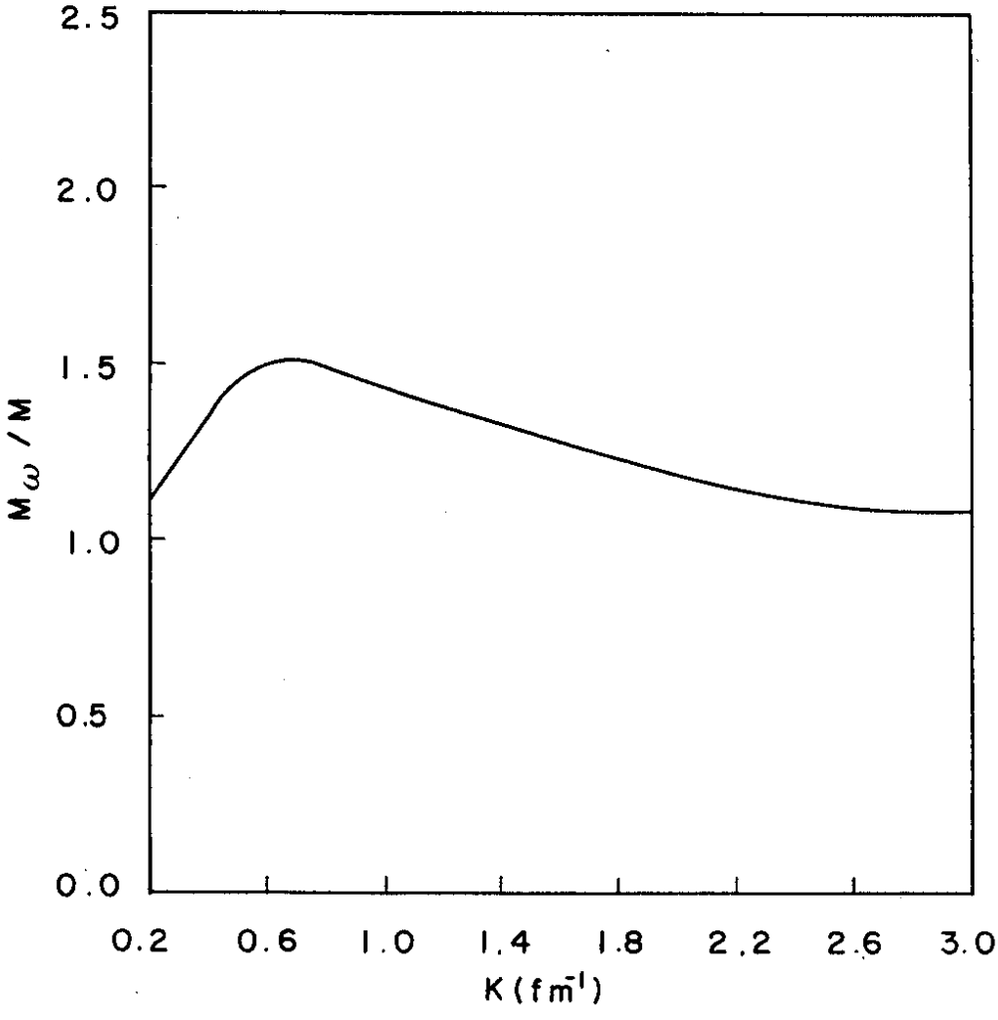
2.5
2.0
1.5
1.0
0.5
0.0
M_ω / M
0.2
0.6
1.0
1.4
1.8
2.2
2.6
3.0
$K(fm^{-1})$

fig. 11

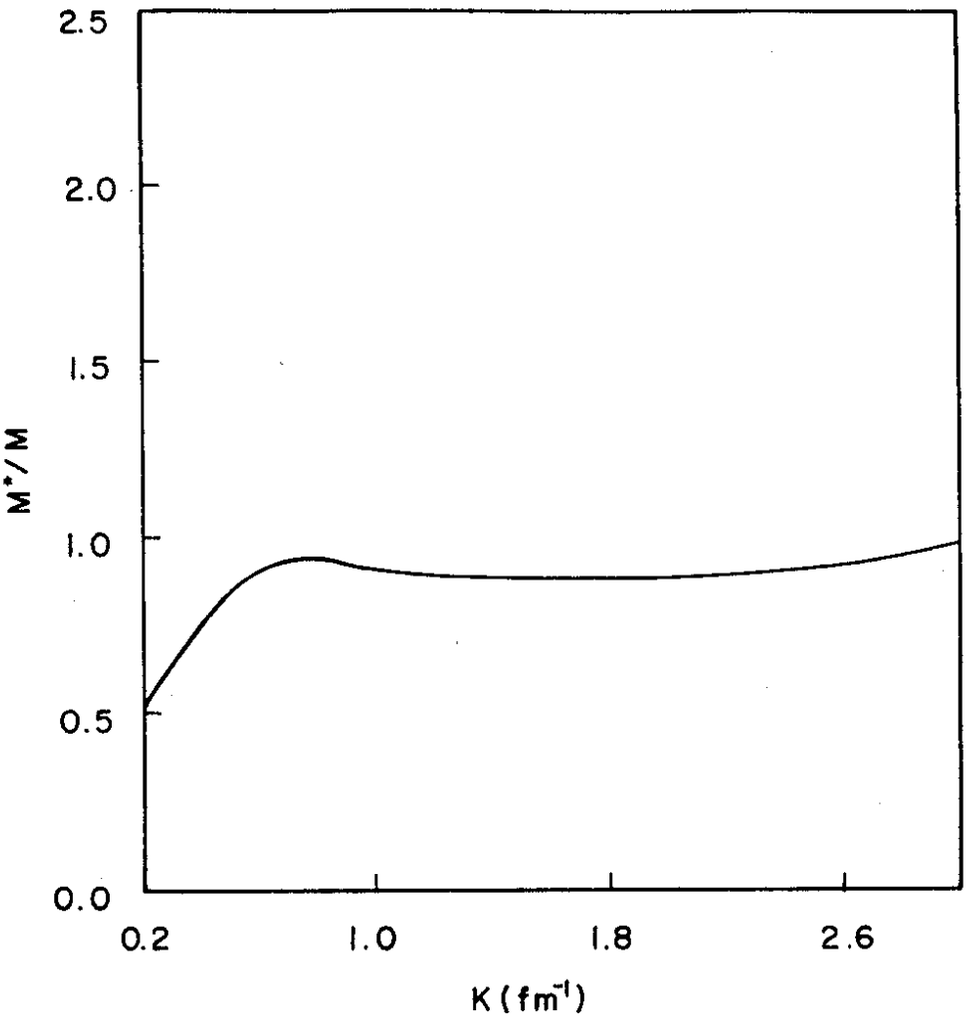
2.5
2.0
1.5
1.0
0.5
0.0
M*/M
0.2
1.0
1.8
2.6
K (fm⁻¹)

fig. 13

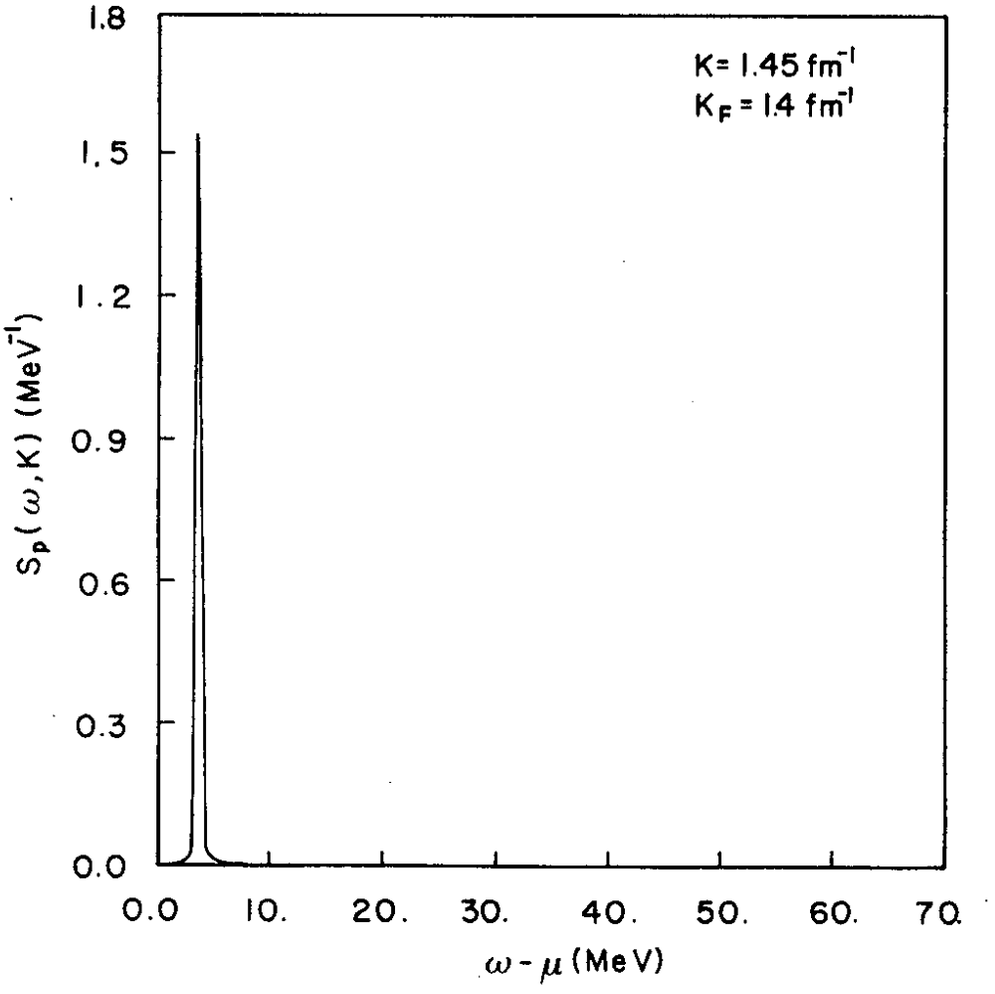
K= 1.45 fm⁻¹
K_F = 1.4 fm⁻¹
1.8
1.5
1.2
0.9
0.6
0.3
0.0
S_p(ω,K) (MeV⁻¹)
0.0
10.
20.
30.
40.
50.
60.
70.
ω - μ (MeV)

fig 14

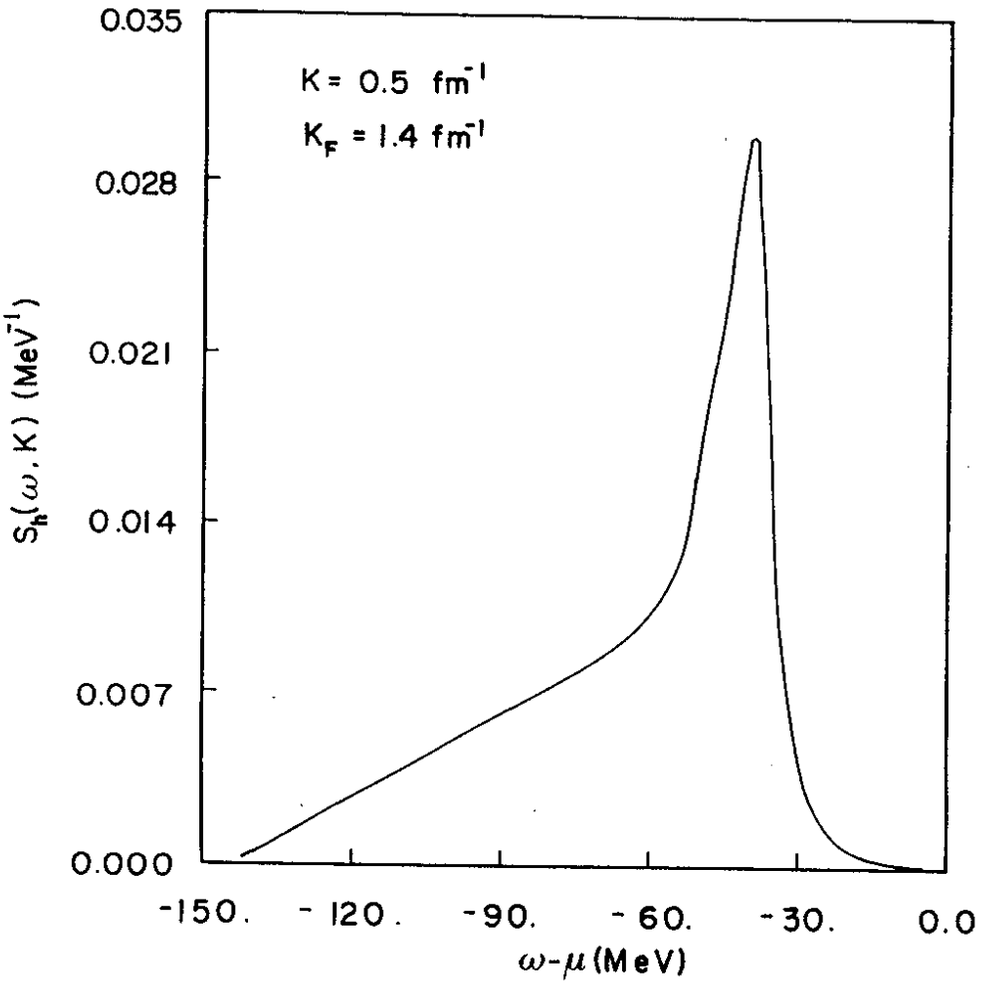
0.035
0.028
0.021
0.014
0.007
0.000
K = 0.5 fm⁻¹
K_F = 1.4 fm⁻¹
S_h(ω, K) (MeV⁻¹)
-150.
-120.
-90.
-60.
-30.
0.0
ω-μ (MeV)

fig. 16

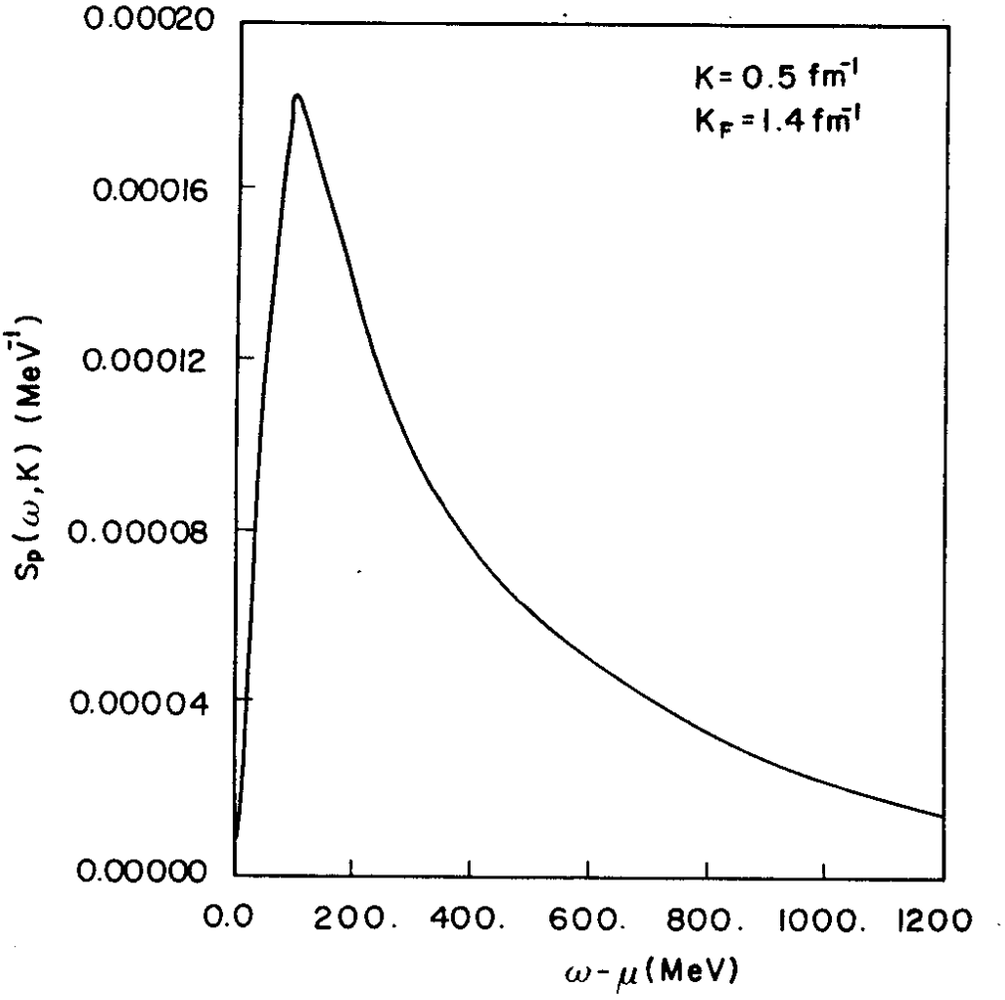
0.00020
0.00016
0.00012
0.00008
0.00004
0.00000
K = 0.5 fm⁻¹
K_F = 1.4 fm⁻¹
S_p(ω, K) (MeV⁻¹)
0.0
200.
400.
600.
800.
1000.
1200
ω-μ (MeV)

fig. 15

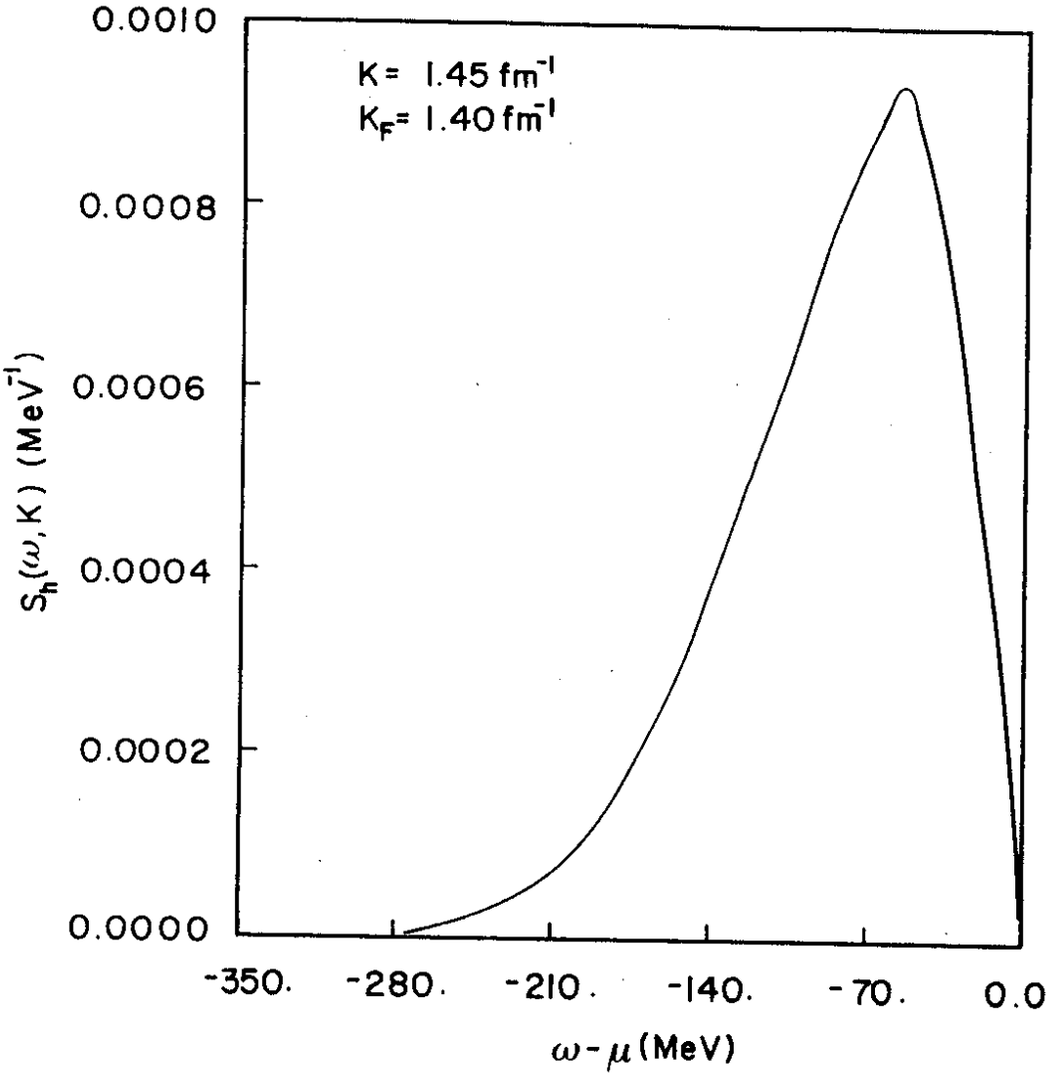
0.0010
0.0008
0.0006
0.0004
0.0002
0.0000
K = 1.45 fm⁻¹
K_F = 1.40 fm⁻¹
S_h(ω, K) (MeV⁻¹)
-350.
-280.
-210.
-140.
-70.
0.0
ω - μ (MeV)

fig. 17